

# Retrieval of Profile Information from Airborne Multi Axis

## UV/visible Skylight Absorption Measurements

Marco Bruns<sup>1</sup>, Stefan A. Buehler<sup>1</sup>, John P. Burrows<sup>1</sup>,  
Klaus-Peter Heue<sup>2</sup>, Ulrich Platt<sup>2</sup>, Irene Pundt<sup>2</sup>, Andreas  
Richter<sup>1</sup>, Alexej Rozanov<sup>1</sup>, Thomas Wagner<sup>2</sup>, Ping Wang<sup>1</sup>

<sup>1</sup>*Institute of Environmental Physics, University of Bremen,*

*P.O. Box 33 04 40, 28359 Bremen, Germany and*

<sup>2</sup>*Institute of Environmental Physics, University of Heidelberg,*

*Im Neuenheimer Feld 229, 69120 Heidelberg, Germany*

## Abstract

A recent development in ground-based remote sensing of atmospheric constituents by UV/visible absorption measurements of scattered light is the simultaneous use of several horizon viewing directions in addition to the traditional zenith-sky pointing. The different light paths through the atmosphere enable the vertical distribution of some atmospheric absorbers such as NO<sub>2</sub>, BrO or O<sub>3</sub> to be retrieved. This approach has recently been implemented on an airborne platform. This novel instrument called Airborne MultiAXis Differential Optical Absorption Spectrometer, AMAXDOAS, has been flown for the first time.

In this study, the amount of profile information that can be retrieved from such measurements is investigated for the trace gas NO<sub>2</sub>. Sensitivity studies on synthetic data are performed for a variety of representative measurement conditions including two wavelengths, one in the UV and one in the visible, two different surface spectral reflectances, various lines of sight (LOS), and for two different flight altitudes.

The results demonstrate that the AMAXDOAS measurements contain useful profile information, mainly at flight altitude and below the aircraft. Depending on wavelength and LOS used, the vertical resolution of the retrieved profiles is as good as 2 km near flight altitude. Above 14 km the profile information content of AMAXDOAS measurements is sparse. Airborne multiaxis measurements are thus a promising tool for atmospheric studies in the troposphere and the UTLS region.

*OCIS codes:* 000.3860, 010.1290, 010.1310, 010.7030, 280.1120, 300.6540.

## 1. Introduction

Since the early 1970's ground-based measurements of the ultraviolet and visible light scattered from the zenith sky have been used to determine the absorptions and thereby the atmospheric column densities of various trace gases (e.g.  $\text{O}_3$ ,  $\text{NO}_2$ ,  $\text{BrO}$ ,  $\text{OClO}$ , ...) by several research groups e.g.<sup>1-5</sup>. These measurements identify specific absorption features using the well known Differential Optical Absorption Spectroscopy (DOAS) method<sup>6</sup>. The typical quantity derived from such measurements is a differential slant column density, that is the difference of the integrated column of molecules along the different light paths through the atmosphere. This is converted to a vertical column by a so-called air mass factor.

A more relevant quantity is the atmospheric profile of a trace gas. Noxon et. al.<sup>7</sup> were the first to estimate the profile information contained in slant column measurements. Later McKenzi et. al.<sup>8</sup> used the weighted Chahine inversion, an iterative method that requires a convergence constraint to retrieve vertical  $\text{NO}_2$  profiles. Preston et. al.<sup>9,10</sup> used the Optimal Estimation method to retrieve  $\text{NO}_2$  profiles from ground-based UV/visible zenith skylight absorption measurements at different SZA. The vertical resolution of such profiles is relatively low, and up to now profile retrievals were only attempted for  $\text{NO}_2$ . Vertically resolved measurements would also be of interest for  $\text{BrO}$  to investigate the presence of  $\text{BrO}$  in the boundary layer and in the free troposphere and its role in catalytic cycles removing  $\text{O}_3$ <sup>11-13</sup>. Airborne UV/visible zenith sky absorption measurements have been performed since the 1980's<sup>14-21</sup>. The experimental setups in these works apply zenith sky absorption measurements to retrieve trace gas columns. Petritoli et. al.<sup>22</sup> have demonstrated that by using an horizon pointing (off-axis) measurement, the retrieval of in-situ information near flight altitude is possible. More recently, Melamed et. al.<sup>23</sup> have used zenith and nadir lines of sight to show the separation of the total column in columns below and above the aircraft.

For the validation of measurements from the SCIAMACHY<sup>24</sup> instrument on board of ENVISAT, the Airborne MultiAxis DOAS instrument (AMAXDOAS)<sup>25</sup> was developed, that takes simultaneous measurements of UV/visible sky absorptions at different lines of sight (LOS) pointing above and below the aircraft. The main focus of the AMAXDOAS measurements is the retrieval of stratospheric and tropospheric columns by using the zenith-sky and nadir viewing directions at a flight altitude close to the tropopause. However, the additional viewing directions are included to investigate the possibility to derive information on the vertical distribution of the absorbers. This is similar to the approach used in ground-based multiaxis measurements<sup>26,27</sup>, which resolve the lower troposphere. More independent pieces of information are expected for AMAXDOAS as compared to the ground-based multiaxis DOAS, as a result of the viewing geometry observed from an aircraft.

It should be noted that the geometry, used in these studies (several LOS measured at one SZA), differs from that used in previous profiling studies, where measurements at one LOS but various SZA are performed, and the variation of scattering height as a function of SZA is used to extract the profile information from the measurements as shown by Preston et. al.<sup>9,10</sup>. In this study, the information content of airborne multiaxis measurements is evaluated, and sensitivity studies are performed to assess the impact of different parameters on the retrieved profiles. A best case scenario with cloudless clear skies and simplified measurement errors is used. The results of this study provide an upper estimate of profile information, which can be retrieved from real measurements. This study analyzes the AMAXDOAS measurements quantitatively. The results are also qualitatively valid for other airborne DOAS measurements.

## 2. The Measurement Geometry

Before discussing the retrieval theory and the sensitivity studies, a qualitative discussion of the viewing geometry highlights and explains the concept to be exploited by the multiaxis measurements. Fig. 1 a.) shows the measurement geometry of AMAXDOAS measurements assuming single-scattering. The ray coming directly from the sun penetrates the atmosphere and is scattered at a specific altitude. As can be seen in this plot, the light paths after scattering are different, and depend on the LOS. The LOS pointing close to the horizon weighting strongly the altitudes containing the trace gas indicated by the longer path inside gray layers. This feature is used by the method described below to retrieve profile information by combining simultaneous measurements of different directions. The distance of the point of scattering from the aircraft is determined by the visibility. The visibility depends on the wavelength, the density of the atmosphere, the aerosol loading, and in the case of nadir view also the distance to the surface.

The upward looking LOS all see the atmosphere above the aircraft, but in the single-scattering approximation are not influenced by the atmosphere below flight altitude. The height from which most of the measurement signal originates depends strongly on the length it travels through denser areas of the atmosphere close to the aircraft. Therefore LOS pointing near the horizon will retrieve a relatively larger signal from the altitudes near flight altitude than LOS pointing more to the zenith.

All downward looking LOS do see the atmosphere above the aircraft too but in addition also probe the atmosphere below flight altitude. These LOS can be divided into two categories. The first category is for those LOS where radiation is scattered above the earth's surface. We call these LOS the limb mode of the AMAXDOAS instrument. For such LOS the largest part of the measurement signal is coming from the tangent height. The different tangent

heights for different LOS yield the profile information in the measurements. The tangent height is the lowest altitude the LOS penetrate due to the spherical shape of the earth. For the single scattering approximation such LOS do not see the atmosphere below that altitude. The second category of LOS include those viewing directions where radiation is scattered close to or at the earth's surface. We call these LOS the nadir mode of the AMAXDOAS instrument. As all these LOS probe all altitudes below the aircraft, the information content of the profile is small and only based on different amounts of scattering depending on the viewing angle. In general these explanations are valid for both the visible and the UV wavelength regions. In the UV the larger extinction by Rayleigh scattering reduces the visibility. More LOS will then act as limb LOS and potentially add profile information below the aircraft.

The radiative modeling used in the quantitative studies reported below includes full multiple scattering and is not limited to the simple assumptions made here.

### **3. The Retrieval Method**

The profile retrieval method used in this work is based on Preston et. al.<sup>9,10</sup>. The retrieval method is modified for the application to airborne UV-visible absorption measurements. The modified method retrieves the profile information using various lines of sight at the same solar zenith angle, whereas the original method retrieves the profile information using only one line of sight but various solar zenith angles [see Fig. 1 b.)].

This retrieval method requires a forward model to calculate the measurement quantity. In the case of DOAS retrievals these are not the radiances but the slant columns for a given trace gas vertical profile. For the simulation of the slant columns, the radiative transfer model SCIATRAN<sup>31</sup> is used. SCIATRAN is a full spherical radiative transfer model taking into account refraction and multiple scattering. It is able to calculate the radiance in specific

lines of sight for a specific flight altitude. The radiances produced by the radiative transfer model are used to calculate air mass factors:

$$AMF(\lambda, j) = \frac{1}{VOD(\lambda, j)} \ln \left( \frac{I(\lambda, gas\ j = OFF)}{I(\lambda, gas\ j = ON)} \right) \quad (1)$$

$VOD(\lambda, j)$  is the vertical optical depth of trace gas  $j$  at wavelength  $\lambda$ ,  $I(\lambda, \text{where gas } j = \text{off})$  is the intensity (radiance) at wavelength  $\lambda$  without trace gas  $j$ , and  $I(\lambda, \text{gas } j = \text{on})$  is the intensity (radiance) at wavelength  $\lambda$  with trace gas  $j$ .

The vertical columns (VC) are converted into simulated slant columns (SC) using the air mass factors of eq. (1).

$$SC = AMF \cdot VC \quad (2)$$

In the sensitivity studies, the SC is being computed using one AMF representative of the spectral window. While this might not always be appropriate for the retrieval of real data, it does not introduce any uncertainties in self-consistent model studies as those discussed here.

#### 4. The Retrieval Theory

A set of slant columns at a certain SZA using different LOS contains information about the vertical distribution of a specific trace gas in the atmosphere. To analyze the quality of the information for profile retrieval the characterization of a retrieval method from Rodgers<sup>28–30</sup> is used. This characterization includes a formal treatment of errors. A set of measurements  $\mathbf{y}$  can be related to a vertical profile  $\mathbf{x}$  by a forward model  $F$ <sup>29</sup>.

$$\mathbf{y} = F(\mathbf{x}, \mathbf{b}) + \epsilon \quad (3)$$



where  $\mathbf{b}$  is the vector of the forward model parameters and  $\epsilon$  is the sum of the measurement error and the model error. In our case,  $\mathbf{y}$  is a vector of slant columns as a function of LOS, and  $\mathbf{x}$  is the vertical profile of the trace gas of interest. The profile  $\mathbf{x}$  - a continuous function in the real atmosphere - has to be sampled discretely by the retrieval algorithm and is therefore presented as a vector. Eq. 3 can be rewritten in a linearized form<sup>28</sup>:

$$\Delta \mathbf{y} = \mathbf{K} \Delta \mathbf{x} \quad (4)$$

where

$$\mathbf{K} = \frac{d\mathbf{y}}{d\mathbf{x}} \quad (5)$$

The rows of the  $\mathbf{K}$  matrix represent the weighting functions, and each row corresponds to a different measurement. Each LOS is considered as a single measurement. The weighting functions describing this problem contain the dependence of the slant columns on the vertical profile for each LOS. In other words: the weighting functions give the change of the slant column when varying the VMR of the profile by a certain amount at a certain altitude.

There is no unique solution to the inversion of eq. 4, because the problem is ill-posed with a condition-number  $\kappa$ . The latter is calculated by doing a singular value decomposition of matrix  $\mathbf{K}$ .  $\kappa$  is the ratio of the largest and the smallest singular values. If  $\kappa$  is of the order of  $10^6$  or larger the problem is generally considered to be ill-posed. In the case of scenario 1 (see Tab.1)  $\kappa$  is of the order of  $10^{29}$ . To reduce the amount of possible solutions the Optimal Estimation Method described by Rodgers<sup>28-30</sup> adds a priori information. A requirement for the Optimal Estimation method to be used is linearity or moderate non-linearity of the problem. The retrieval problem for trace gas skylight absorption measurements is nearly linear because most trace gases (e.g.  $\text{NO}_2$ ) are optically thin (i.e. absorptions smaller than

2%). In this study the Maximum a Posteriori (MAP) solution is chosen<sup>30</sup>. This method calculates the retrieved profile as follows:

$$\hat{\mathbf{x}} = \left( \mathbf{K}^T \mathbf{S}_\epsilon^{-1} \mathbf{K} + \mathbf{S}_a^{-1} \right)^{-1} \left( \mathbf{K}^T \mathbf{S}_\epsilon^{-1} \mathbf{y} + \mathbf{S}_a^{-1} \mathbf{x}_a \right) \quad (6)$$

where  $\mathbf{K}$  is the weighting function matrix,  $\mathbf{S}_\epsilon$  is measurement error covariance matrix,  $\mathbf{S}_a$  is the arbitrary error covariance matrix of the a priori vector,  $\mathbf{y}$  is the measurement vector, and  $\mathbf{x}_a$  is the a priori profile information.

To characterize the retrieved profile more precisely, the contribution function matrix  $\mathbf{D}$  is introduced. This represents the sensitivity of the retrieved profile to the changes of the slant columns:

$$\mathbf{D} = \frac{\partial \hat{\mathbf{x}}}{\partial \mathbf{y}} = \mathbf{S}_a \mathbf{K}^T \left( \mathbf{K} \mathbf{S}_a \mathbf{K}^T + \mathbf{S}_\epsilon \right)^{-1} \quad (7)$$

where  $\mathbf{K}^T$  is the transposed weighting function matrix  $\mathbf{K}$  and  $\mathbf{S}_\epsilon$  is the measurement error covariance matrix. The contribution functions indicate the variation of the retrieved profile when changing the slant column at a given LOS by a certain amount of molecules per  $\text{cm}^2$ . The retrieved profile can be thought of as a weighted average of the true and the a priori profiles. The averaging kernel matrix supplies the weights for the true profile.

$$\mathbf{A} = \mathbf{D} \mathbf{K} \quad (8)$$

A change in the real atmospheric profile by a certain amount of molecules per  $\text{cm}^3$  in a specific altitude causes a change of a certain amount of molecules per  $\text{cm}^3$  in the retrieved profile at all altitudes represented by a function, the averaging kernel for this specific altitude. The vertical resolution of the profile retrieval is determined from the averaging kernels. Rodgers

defined the vertical resolution of a profile retrieval at a specific altitude as the Full Width Half Maximum (FWHM) value of the corresponding averaging kernel <sup>30</sup>.

The radiative transfer model SCIATRAN is used to calculate the weighting functions for this study. These weighting functions give the absolute change in intensity for a relative change of 100% of a parameter, for example NO<sub>2</sub> in layer 15. However, for AMAXDOAS one is more interested in a weighting function that indicates the change in slant column for a change in say NO<sub>2</sub> at layer 15. Fortunately, for an optically thin atmosphere, the weighting functions as calculated by SCIATRAN can easily be converted into weighting functions for the slant columns. After calculating the contribution functions using eq. 7 the averaging kernels can be calculated using eq. 8 with the weighting functions representing  $\mathbf{K}$ .

## 5. Retrieval Error Analysis

The total error of the retrieved profile can be separated into three components. According to Rodgers<sup>30</sup> the total error of the profile retrieval is the difference between the retrieved and the true profile. Due to error propagation the error covariance matrix of the total error can be written as:

$$\mathbf{S}_{tot} = \mathbf{S}_n + \mathbf{S}_m + \mathbf{S}_f \quad (9)$$

$\mathbf{S}_n$  is the a priori error covariance matrix,  $\mathbf{S}_m$  is the measurement error covariance matrix or retrieval noise, and  $\mathbf{S}_f$  is the forward model error covariance matrix. The last error component will not be considered in this work because the error produced by the forward model SCIATRAN is less than 2% for LOS with tangent heights up to 30 km<sup>31</sup>.

The a priori error covariance matrix  $\mathbf{S}_n$  can be calculated as:

$$\mathbf{S}_n = (\mathbf{A} - \mathbf{I})\mathbf{S}_a(\mathbf{A} - \mathbf{I})^T \quad (10)$$

where  $\mathbf{S}_a$  is the error covariance matrix of the a priori profile. Rodgers<sup>30</sup> refers to the a priori error as smoothing error, as this covariance matrix  $\mathbf{S}_n$  corresponds to portions of profile space the measurements cannot see. In our case those portions are the altitudes in the stratosphere, and small scale variations obscured by the limited altitude resolution of the profile retrieval.

Another source of error in real applications is the pointing accuracy of the LOS. A high pointing accuracy is difficult to achieve because of the intrinsic pitch and roll of an aircraft in flight. The matter of pointing accuracy will be dealt with in the sensitivity studies below. The measurement error covariance matrix  $\mathbf{S}_m$  can be calculated as:

$$\mathbf{S}_m = \mathbf{D}\mathbf{S}_\epsilon\mathbf{D}^T \quad (11)$$

where  $\mathbf{S}_\epsilon$  is the covariance matrix of the measurement error and  $\mathbf{D}$  is the contribution function matrix. The measurement error is due to noise in the measurements propagating into the retrieval. The contribution function matrix maps the measurement error into the profile space.

## 6. Sensitivity Studies

To assess the amount of profile information contained in AMAXDOAS measurements, slant columns are being simulated for a number of different scenarios and a retrieval performed using the method described in the previous sections. The results are discussed by evaluating the averaging kernels, weighting functions and retrieval errors. An overview of the different scenarios that are being studied is given in Tab. 1. Briefly, the influence of wavelength,

surface spectral reflectance (from now on referred to as albedo), flight altitude and also the choice of LOS and pointing accuracy is being investigated. While the choice of specific parameters (the standard LOS:  $0^\circ$ ,  $60^\circ$ ,  $80^\circ$ ,  $85^\circ$ ,  $88^\circ$ ,  $92^\circ$ ,  $95^\circ$ ,  $100^\circ$ ,  $120^\circ$ ,  $180^\circ$ ; a flight altitude of 10 km; and wavelengths of 350 and 500 nm) is based on the set-up and operation of the AMAXDOAS instrument, the results are valid in general and not restricted to this experiment. Also, the discussion is focused on the case of  $\text{NO}_2$  retrieval but can readily be applied to other trace gases taking into account the differences in the absorption cross sections and wavelength used.

In this study different retrieval grids are used in order to take into account different vertical resolutions. The first retrieval grid is used for a flight altitude of 10 km and has points at 0 km, 1 km, 3 km, ..., 39 km. At a flight altitude of 2 km a second retrieval grid with points at 0 km, 0.2 km, ..., 4 km, 5 km, 7 km, 9 km, ..., 39 km is used.

For these studies a low aerosol scenario from LOWTRAN<sup>33,34</sup> is chosen, using a visibility in the boundary layer (0 to 2 km) of 23 km, a maritime aerosol type, and 80% humidity. In the free troposphere (2 to 10 km) the visibility is set to 23 km and the humidity to 80%. In the stratosphere the aerosol loading is that of a background scenario. For all studies, a cloud free scenario is assumed.

The meteorological data used in the radiative transfer model are taken from the 3-dimensional chemical transport model SLIMCAT<sup>35</sup>. A mid-latitude spring scenario and a fixed SZA of  $51.6^\circ$  is used. From the output of the radiative transfer model only data with a  $90^\circ$  relative azimuth angle with respect to the sun is taken into account, assuming there are no horizontal inhomogeneities in the trace gas abundance.

For this retrieval method different LOS are crucial. The following 10 different LOS are assumed:  $0^\circ$  (nadir),  $60^\circ$ ,  $80^\circ$ ,  $85^\circ$ ,  $88^\circ$ ,  $92^\circ$ ,  $95^\circ$ ,  $100^\circ$ ,  $120^\circ$ , and  $180^\circ$  (zenith).

The sensitivity studies are done for  $\text{NO}_2$ . To perform the sensitivity studies, appropriate values for the a priori ( $\sqrt{\mathbf{S}_a}$ ) and measurement error ( $\sqrt{\mathbf{S}_\epsilon}$ ) have to be assumed. Since the measured slant columns will be in the order of  $10^{16}$  molec/cm<sup>2</sup> to  $1.5 \cdot 10^{16}$  molec/cm<sup>2</sup>, a standard deviation of  $10^{15}$  molec/cm<sup>2</sup> is a realistic measurement error. A good DOAS instrument is able to measure a differential optical depth as small as  $3 \cdot 10^{-4}$  with a reasonable signal to noise ratio of 2. Using the differential cross section of  $\text{NO}_2$  near 500 nm of  $2.5 \cdot 10^{-19}$  cm<sup>2</sup>/molecule the smallest slant column measurable with this instrument is calculated to be  $1.2 \cdot 10^{15}$  molecules/cm<sup>2</sup>.

The maximum mixing ratio of the  $\text{NO}_2$  profile is in the order of 9 ppbv. In this case a standard deviation of 1 ppbv as a priori error seems to be reasonable.

## 7. Results

In Fig. 2.1 the averaging kernels for scenario 1 are shown. This scenario assumes a flight altitude of 10 km, a wavelength of 350 nm, and an albedo of 0.1. A first look at the averaging kernels reveals a large sensitivity of the profile retrieval near flight altitude. As is discussed above, the averaging kernels at 350 nm cannot be understood by considering only the tangent heights for every LOS. This is because of the limited visibility at 350 nm.

There are two distinctive averaging kernels (9 and 11 km) suggesting a very high sensitivity and a vertical resolution of 2.0 and 2.1 km near the flight altitude. Going further down towards the surface the averaging kernels broaden. In contrast to the 9 km averaging kernel the 1 km averaging kernel has a FWHM value of 4.9 km. The changing peak altitudes and FWHM values for the averaging kernels can be understood considering the limited visibility of the atmosphere in the UV at 350 nm. Good vertical resolution will be achieved if the average light paths through different altitude layers differ strongly. This is the case for the layer close to flight altitude, which is penetrated differently by the individual viewing

directions. To understand this pattern of averaging kernels it is necessary to analyze the weighting functions. The section dealing with the retrieval theory described the weighting functions as sensitivity of the measurements as a function of altitude. The maximum of the weighting functions are indicators for the altitude from which most of the information for a given LOS is coming from. The weighting functions for scenario 1 are shown in Fig. 3.1. The weighting functions for the downward looking LOS peak in different altitudes. This suggests, that different LOS are sensitive to different altitudes.

Above the aircraft the vertical resolution of the averaging kernels decreases. The FWHM of the 11 km averaging kernel is 2.1 km, whereas the FWHM value of the 13 km averaging kernel is 3.7 km. All averaging kernels above flight altitude peak at 13 km except for the 11 km averaging kernel. The weighting functions of Fig. 3.1 confirm the information given by the averaging kernels. The sensitivity of the upward looking LOS to altitudes above 13 km is small and does not contain profile information.

As discussed in the previous section the SZA for these sensitivity studies is  $51.6^\circ$ . Two additional SZA ( $20^\circ$  and  $80^\circ$ ) are tested but results are not presented here as the general behavior of the averaging kernels does not change.

Fig. 4 shows the retrieval errors for different scenarios resulting from the a priori and measurement error described above. The total retrieval error  $(S_n + S_m)^{-0.5}$  is a measure of quality of the retrieval. A small total error indicates a retrieval of high quality.

A comparison with the retrieval error of a profile retrieval using a retrieval grid with 1 km step size (not shown here) reveals that the retrieval error decreases significantly when the retrieval grid step size is increased. There appears to be sufficient information in the measurements that the use of a retrieval grid with 2 km step size seems to be reasonable.

#### *A. Influence of the Wavelength on the Retrieval:*

In this investigation two wavelengths are used, one in the UV (350 nm) and one in the visible wavelength region (500 nm). The averaging kernels of scenario 1 (see Fig. 2.1) and scenario 2 (see Fig. 2.2) are compared. The overall behavior of the averaging kernels at 500 nm is basically the same as at 350 nm.

There are however a few exceptions. The first exception is that the vertical resolution of the 9 km averaging kernel decreases significantly (4.5 km instead of 2.0 km in scenario 1). The second exception is that the 0 km and 5 km averaging kernels have a significantly increased vertical resolution. Compared to scenario 1 the vertical resolution for the 0 km averaging kernel increased from 3.5 to 1.3 km. The vertical resolution for the 5 km averaging kernel increased from 4.9 to 2.4 km. The weighting functions for scenario 2 are plotted in Fig. 3.2 and it can be seen that there are no two LOS, that can resolve the layer between flight altitude and 5 km explaining the significantly decreased vertical resolution at 9 km.

The third exception is, that the 0 km averaging kernel has a much larger value compared to the same averaging kernel for 350 nm. This feature suggests a higher sensitivity of the 500 nm measurements in the lower troposphere, as is expected as a result of the reduced importance of Rayleigh scattering at this wavelength.

As can be seen in Fig. 2.2 the vertical resolution at 500 nm is lower than at 350 nm between 7 and 9 km altitude, but it is higher at an altitude of 5 km. This result is confirmed by the retrieval errors shown in Fig. 4.2. For 500 nm, the retrieval error between 7 and 9 km altitude is larger than at 350 nm but smaller than that at 350 nm at 5 km altitude.

#### *B. Influence of Albedo on the Retrieval*

To investigate the influence of albedo or surface spectral reflectance, the averaging kernels for albedos of 0.1 and 0.9 respectively are considered for the 2 wavelengths (350 and 500 nm).



For scenario 4 at 500 nm (see Fig. 2.4) and an albedo of 0.9, there is no significant change compared to scenario 2 at 500 nm and an albedo of 0.1. However, in the UV at 350 nm, the 0 km averaging kernel increases by 50% (see Fig. 2.3). The averaging kernels for altitudes above 0 km do not change when the albedo is changed from 0.1 to 0.9. The same holds for the averaging kernels above the aircraft. This can be explained by taking into account the enhancement of multiple scattering as a result of the larger number of reflected photons at the surface in the UV wavelength region. The enhanced multiple scattering is limited to the lower altitudes close to the surface, because multiple scattering is occurring and most likely in parts of the atmosphere having a higher density. The overall result of this study is that large albedo will increase the sensitivity of UV measurements in the surface layer but apart from that there is little influence on the profile information of the measurements.

### *C. Influence of Additional Lines of Sight on the Retrieval:*

To investigate the usefulness of having more different LOS (see Fig. 2.6) the calculations for two additional LOS ( $89^\circ$  and  $91^\circ$ ) are included at 500 nm and compared to scenario 2 (see Fig. 2.2). For scenario 6 the averaging kernels 7 and 9 km below the aircraft peak in different altitudes compared to those in scenario 2. The weighting functions (Fig. 3.6) explain this behavior. For the  $89^\circ$  LOS, the retrieval obtains information exclusively from the altitudes near 9 km, because the majority of the absorption signal originates from these altitudes due to a tangent height of 9 km for the  $89^\circ$  LOS. The  $88^\circ$  LOS weighting function is the same as in scenario 2. Therefore, as a result of the additional LOS, additional profile information about higher altitudes is gathered. For 350 nm (see Fig. 3.5) there is no difference in the weighting functions of the  $88^\circ$ , and the  $89^\circ$  LOS. Thus no increase in the vertical resolution is observed. The fact that the additional LOS do not increase the profile resolution at 350 nm results from the limited visibility at 350 nm. Above the aircraft the averaging kernels do

not change compared to scenario 1.

Fig. 3.6 shows that the vertical resolution at 500 nm can be improved when using additional LOS at  $89^\circ$  and  $91^\circ$ . Analysis of the retrieval errors in Fig. 4.6 confirms the improvement of the resolution at 500 nm due to the smaller retrieval error compared to scenario 2.

#### *D. Influence of the Flight Altitude on the Retrieval*

In this part of the study calculations for a flight altitude of 2 km are compared to those for 10 km flight altitude. Again, two cases have to be considered. The first case is the scenario 7 calculated for a wavelength of 350 nm, the second one is calculated for a wavelength of 500 nm. As can be seen in Fig. 5.7a and b for scenario 7, the averaging kernels calculated for this flight altitude do not peak as distinctively as they did for the 10 km flight altitude. This is to be expected given the vertical resolution of 2 km that could be achieved at 10 km. Above and below the flight altitude, the peak values of the averaging kernels decrease rapidly. This fact and a study of the retrieval error (not shown) suggest that the measurement at 2 km flight altitude is not containing much profile information. In summary measurements at 2 km flight altitude yield profile information only at flight altitude in addition to the columns below and above the aircraft. The averaging kernels above the aircraft contain less profile information compared to measurements taken at 10 km flight altitude in the UV.

The second case is the scenario 8 calculated for a wavelength of 500 nm. As can be seen in Fig. 5.8a and b, the averaging kernels are nearly identical to the UV case. The difference of averaging kernels between the two wavelengths is small, because the distances from the aircraft to the surface for almost all LOS for both wavelengths are within the visibility range of the model atmosphere. The main result of this study is that only a column above and beneath the aircraft can be retrieved.

*E. What is the optimum LOS setup?*

This question has two parts. The first is addressing the optimum number of LOS required, when retrieving a profile with a certain resolution. Rodgers deals with this part of the question by the use of prior constraints. To make the inversion problem well-posed, 'a discrete representation with fewer parameters than the number of degrees of freedom of the measurements' is needed as required by the maximum a posteriori method (<sup>30</sup>, chapter 10). For our example this translates to: if the retrieved profile below the aircraft has 5 points, at least 5 measurements (downward looking LOS) are needed to make the problem well-posed. The second part of the question deals with the selection of LOS for a specific setup. This can be answered by selecting the LOS in such a way that for each layer in the retrieval grid one limb measurement is taken that has the appropriate tangent height. For the retrieval grid of 0 km, 1 km, 3 km, ..., 9 km the according LOS would be: 86.8°, 87.0°, 87.3°, 87.7°, 88.2°, and 89.0°.

In practice this approach is not very useful because the required pointing accuracy of 0.1° is difficult to realize. Therefore a downsized version of this approach will be tested. Instead of 18 LOS required for all tangent heights from 0 to 9 km only 12 LOS will be used. This scenario is realized by using the LOS 0°, 80°, 85°, 88°, 89°, 91°, 92°, 95°, 100°, and 180° plus the LOS 87° and 93°. At 500 nm, the comparison of the 18 LOS study (not shown here) to the 12 LOS study reveals an increase of 15% of the maximum vertical resolution below flight altitude [max. VR (18 LOS) is 2.0; max. VR (12 LOS) is 2.3]. This change is small compared to the 83% increase in maximum vertical resolution below flight altitude when changing the LOS setup from scenario 6 to scenario 10 (see Fig. 2.6, Fig. 6.10, and Tab. 2). From this we conclude, that no further information is gathered in going from 12 to 18 LOS. At 350 nm there is practically no difference between the 10 LOS setup and the

12 LOS setup (see Fig. 2.5 and Fig. 6.9). The 18 LOS setup does not increase the maximum vertical resolution below flight altitude. At 350 nm, the 10 LOS setup is already the LOS setup with the best performance. For 500 nm the LOS setup with the best performance is the setup with 18 LOS but for practical reasons the 12 LOS setup is as good as the 18 LOS setup. The retrieval error for the 12 LOS study at 500 nm (see. Fig. 4.10) supports the better performance of the 10 LOS.

#### *F. Influence of the Pointing Accuracy on the Retrieval*

The last part of this investigation deals with the pointing accuracy of the LOS. To test the influence of the pointing accuracy on the retrieval, the retrieval errors are calculated for a profile retrieval of the 12 LOS study and a pointing error is added to each LOS. To characterize the decrease in retrieval quality, the ratio of the retrieval error with and without pointing error is calculated (see Fig. 7). A pointing error of less than  $1^\circ$  does not change the retrieval error significantly at 350 nm as shown in Fig. 7 a.). The largest relative changes occur at altitudes with small retrieval errors, and therefore the absolute retrieval quality is not decreased significantly. At 500 nm a pointing accuracy of better than  $1^\circ$  is very important as can be seen in Fig. 7 b.) to d.). The same retrieval quality as for 350 nm is achieved, when a pointing accuracy of better than  $0.1^\circ$  is assumed. For real flights the pointing accuracy for all LOS is known a posteriori as good as  $0.01^\circ$ .

## **8. Conclusions**

Sensitivity studies are being performed to determine the amount of profile information contained in airborne UV/vis skylight absorption measurements. The result of this work is that there is indeed valuable profile information in airborne multi axis UV/vis skylight absorption measurements. The vertical resolution of the profile retrieval depends on the LOS setup,

the flight altitude, and the wavelength. Airborne multiaxis measurements have an excellent sensitivity in the troposphere and upper troposphere/lower stratosphere. Tab. 2 shows the vertical resolution of the profile retrieval for each scenario.

The investigation of the influence of the wavelength on the retrieval indicates that measurements in the UV (350 nm) contain profile information with a higher vertical resolution between 5 and 10 km altitude than measurements at 500 nm. For 350 nm, the sensitivity studies show a vertical resolution of 2.0 km near flight altitude. Below 7 km altitude and above the aircraft the vertical resolution decreases to 4.9 km. At 500 nm, the vertical resolution of 4.5 km is much lower at 9 km altitude compared to 2.0 km at 350 nm at 9 km altitude. In contrast, the vertical resolution is significantly better at 1 and 5 km altitude. Above the aircraft the vertical resolution at 500 nm is lower at 350 nm by as much as 25%. When comparing the averaging kernels for high and low albedo, it turns out that the differences are small at both wavelengths with exception of the very small UV averaging kernel at the surface. Albedo is therefore a critical parameter for the retrieval in the lower troposphere near the surface.

Additional lines of sight near the horizon will improve the profile resolution near flight altitude at 500 nm whereas the profile resolution at 350 nm remains basically the same (see Tab. 2). This can be seen by comparing figures 3.2 and 3.6 and figures 2.2 and 2.6. With additional lines of sight at 500 nm the resolution of the retrieved profile will be as good as or better than the resolution of scenario 1. However, in practice it is difficult to achieve the necessary pointing accuracy close to the horizon on a moving aircraft and the potential improvement might not be possible in practice.

The main result obtained in the study of the influence of the flight altitude is that at lower altitudes little profile information can be retrieved from the measurements for either

wavelength. The reason is, that most of the profile information comes from the downward looking limb LOS. For lower flight altitudes the number of LOS in limb mode decreases rapidly assuming a fixed LOS setup. Still, near flight altitude enhanced sensitivity is achieved adding some vertical resolution to the measurements. In practice, flying at different altitudes does provide profile information since these studies show that the best profile information can be extracted from the flight altitude region.

Concerning the requirements on pointing accuracy, it turns out that a pointing accuracy of  $1^\circ$  is sufficient for measurements at 350 nm but a pointing accuracy of  $0.1^\circ$  is required for measurements at 500 nm.

For practical applications, clouds, horizontal inhomogeneities, and aerosols will introduce further uncertainties and reduce the achievable vertical resolution of the retrieved profile. The combination of two or even more wavelengths contains a large optimization potential, since it is shown that the same LOS using different wavelengths is sensitive to different altitudes of the profile. The sensitivity studies also show that these measurements are most sensitive to profile information close to flight altitude. Therefore combination of measurements at different altitudes, and possibly also at different SZA has the potential of adding profile information, further improving the theoretical vertical resolution. Overall this sensitivity study demonstrates the potential of AMAXDOAS measurements to provide height resolved information on a number of relevant species in the troposphere and the important UTLS region using a relatively simple remote sensing instrument on an airborne platform.

## **9. Acknowledgements**

Part of this work is funded by the "SCIAMACHY Validations Programm" (Förderkennzeichen 50EE0023) by means of the German Ministry of Sciences (BMBF) and the University of Bremen. We would like to thank Kathy Preston and Howard Roscoe for

providing the computer code this work is based on. Last but not least we would like to thank Martin Chipperfield for providing the data of the 3-D SLIMCAT model output. The authors would like to thank two anonymous reviewers for helpful comments and suggestions.

## References

1. A. W. Brewer, C. T. McElroy, and J. B. Kerr, "Nitrogen Dioxide Concentrations in the atmosphere", *Nature*, **246** (5429), 129-133, (1973)
2. J. F. Noxon, "Nitrogen dioxide in the stratosphere and troposphere measured by ground-based absorption spectroscopy", *Science*, **189**, 547-549, (1975)
3. R. L. McKenzi and P. V. Johnston, "Seasonal variations in stratospheric NO<sub>2</sub> at 45°S", *Geophys. Res. Lett.*, **9**, 1255-1258, (1982)
4. J. P. Pommereau and F. Goutail, "O<sub>3</sub> and NO<sub>2</sub> Ground-Based Measurements by Visible Spectrometry during Arctic Winter and Spring 1988", *Geophys. Res. Lett.*, **15**, 891-894, (1988)
5. S. Solomon, A. L. Schmeltekopf, and R. W. Sanders, "On the interpretation of zenith sky absorption measurements", *J. Geophys. Res.*, **92**, 8311-8319, (1987)
6. U. Platt, Differential optical absorption spectroscopy (DOAS), in *Air Monitoring by Spectroscopic Techniques*, Chem. Anal. Ser., vol. 127, edited by M. W. Sigrist, pp. 27-84, John Wiley, New York, 1994.
7. J. F. Noxon, E. C. Whipple Jr., and R. S. Hyde, "Stratospheric NO<sub>2</sub>: 1. Observational method and behavior at mid-latitudes", *J. Geophys. Res.*, **84**, 5047-5065, (1979)
8. R. L. McKenzi, P. V. Johnston, C. T. McElroy, J. B. Kerr, and S. Solomon, "Altitude distributions of stratospheric constituents from ground-based measurements at twilight", *J. Geophys. Res.*, **96**, 15499-15511, (1991)
9. K. E. Preston, "The Retrieval of NO<sub>2</sub> vertical profiles from ground-based Twilight

- UV-visible measurements”, Ph.D. Thesis, Pembroke College, Cambridge, (1995)
10. K. E. Preston, R. L. Jones, and H. K. Roscoe, ”Retrieval of NO<sub>2</sub> vertical profiles from ground-based UV-visible measurements: Method and validation”, J. Geophys. Res., **102**, 19089-19097, (1997)
  11. L. A. Barrie, J. W. Bottenheimer, R. C. Schnell, P. J. Crutzen, and R. A. Rasmussen, ”Ozone destruction and photochemical reactions at polar sunrise in the lower Arctic atmosphere”, Nature, **334**, 138-141, (1988)
  12. A. Richter, F. Wittrock, M. Eisinger, and J. P. Burrows, ”GOME Observations of Tropospheric BrO in Northern Hemispheric Spring and Summer 1997”, Geophys. Res. Lett., **25**, 2683-2686, (1998)
  13. T. Wagner and U. Platt, ”Satellite mapping of enhanced BrO concentrations in the troposphere”, Nature, **395**, 486-490, (1998)
  14. A. Wahner, R. O. Jakoubek, G. H. Mount, A. R. Ravishankara, and A. L. Schmeltekopf, ”Remote Sensing Observations of Nighttime OClO Column During the Airborne Antarctic Ozone Experiment, September 8, 1987”, J. Geophys. Res., **94**, 11405-11411, (1989)
  15. A. Wahner, R. O. Jakoubek, G. H. Mount, A. R. Ravishankara, and A. L. Schmeltekopf, ”Remote Sensing Observations of Daytime Column NO<sub>2</sub> During the Airborne Antarctic Ozone Experiment, August 22 to October 2, 1987”, J. Geophys. Res., **94**, 16619-16632, (1989)
  16. A. Wahner, J. Callies, H.-P. Dorn, U. Platt, and C. Schiller, ”Near UV Atmospheric Absorption Measurements of Column Abundances During Airborne Arctic Stratospheric Expedition, January-February 1989: Technique and NO<sub>2</sub> Observations”, Geophys. Res. Lett., **17**, 497-500, (1990)



17. A. Wahner, J. Callies, H.-P. Dorn, U. Platt, and C. Schiller, "Near UV Atmospheric Absorption Measurements of Column Abundances During Airborne Arctic Stratospheric Expedition, January-February 1989: 3. BrO Observations", *Geophys. Res. Lett.*, **17**, 517-520, (1990)
18. C. Schiller, A. Wahner, H.-P. Dorn, U. Platt, J. Callies, and D. H. Ehhalt, "Near UV Atmospheric Absorption Measurements of Column Abundances During Airborne Arctic Stratospheric Expedition, January-February 1989: 2. OCIO Observations", *Geophys. Res. Lett.*, **17**, 501-504, (1990)
19. R. Brandtjen, T. Klüpfel, D. Perner, and B. M. Knudsen, "Airborne measurements during the European Arctic Stratospheric Ozone Experiment: Observation of OCIO", *Geophys. Res. Lett.*, **21**, 1363-1366, (1994)
20. K. Pfeilsticker and U. Platt, "Airborne measurements during the European Arctic Stratospheric Ozone Experiment: Observation of O<sub>3</sub> and NO<sub>2</sub>", *Geophys. Res. Lett.*, **21**, 1375-1378, (1994)
21. F. Erle, A. Grendel, D. Perner, U. Platt, and K. Pfeilsticker, "Evidence of heterogeneous bromine chemistry on cold stratospheric sulphate aerosols", *Geophys. Res. Lett.*, **25**, 4329-4332, (1998)
22. A. Petritoli, F. Ravegnani, G. Giovanelli, D. Bortoli, U. Bonaf, I. Kostadinov, A. Oulanovsky, "Off-Axis Measurements of Atmospheric Trace Gases by Use of an Airborne Ultraviolet-Visible Spectrometer", *Applied Optics*, **27**, 5593-5599, (2002)
23. M. L. Melamed, S. Solomon, J. S. Daniel, A. O. Langford, R. W. Portmann, T. B. Ryerson, D. K. Nicks, Jr. and S. A. McKeen, "Measuring reactive nitrogen emissions from point sources using visible spectroscopy from aircraft", *J. Environ. Monit.*, **5**, 29-34, (2003)

24. H. Bovensmann, J. P. Burrows, M. Buchwitz, J. Frerick, S. Nol, V. V. Rozanov, K. V. Chance, and A. H. P. Goede, "SCIAMACHY - Mission objectives and measurement modes", J. Atmos. Sci., **56**, (2), 127-150, (1999)
25. T. Wagner, M. Bruns, J.P. Burrows, S. Fietkau, F. Finocchi, K.-P. Heue, G. Hönniger, U. Platt, I. Pundt, A. Richter, R. Rollenbeck, C. von Friedeburg, F. Wittrock, P. Xie, "The AMAXDOAS instrument and its application for SCIAMACHY validation", Proceedings of the 15th ESA Symposium on European Rocket and Balloon Programmes and Related Research (ESA SP-471, August 2001), Biarritz, France, 28-31 May, (2001)
26. G. Hönniger and U. Platt, "The Role of BrO and its Vertical Distribution during Surface Ozone Depletion at Alert", Atmos. Environ., **36**, 2481-2489, (2002)
27. F. Wittrock, H. Oetjen, A. Richter, S. Fietkau, T. Medeke, A. Rozanov, and J. P. Burrows, MAX-DOAS measurements of atmospheric trace gases in Ny-Ålesund, Atmos. Chem. Phys. Discuss., **3**, 6109–6145, (2003)
28. C. D. Rodgers, "Retrieval of atmospheric temperature and composition from remote measurements of thermal radiation", Rev. Geophys., **14**, 609-624, (1976)
29. C. D. Rodgers, "Characterization and error analysis of profiles retrieved from remote sounding measurements", J. Geophys. Res., **95**, **D5**, 5587-5595, (1990)
30. C. D. Rodgers, *Inverse Methods for atmospheric sounding: Theory and Practice*, Series on Atmospheric, Oceanic and Planetary Physics, Vol. 2, (World Scientific Publishing, London, 2000)
31. A. Rozanov, V. Rozanov and J. P. Burrows, "A numerical radiative transfer model for a spherical planetary atmosphere: combined differential integral approach involving the Picard iterative approximation", J. Quant. Spectrosc. Radiat. Transfer, **69**, 491-512, (2001)

- 32. L. C. Marquard, T. Wagner, and U. Platt, "Improved air mass factor concepts for scattered radiation differential optical absorption spectroscopy of atmospheric Species", J. Geophys. Res., **105**, 1315-1327, (2000)
- 33. E. P. Shettle and R. W. Fenn, "Models of the aerosols of the lower atmosphere and the effects of humidity variations on their optical properties", Tech. rep., AFGL-TR-79-0214, Project 7670, Air Force Geoph. Lab., Hanscom AFB, MA, (1979)
- 34. F. X. Kneizys, E. P. Shettle, L. W. Abreu , J. H. Chetwynd, G. P. Anderson, W. O. Gallery, J. E. A. Selby, and S. A. Clough, "Users Guide to LOWTRAN 7", Tech. rep., AFGL-TR-88-0177, (NTIS AD A206773), Air Force Geophysics Laboratory AFGL, Hanscom AFB, MA, (1986)
- 35. M. Chipperfield, "Multiannual simulations with a three-dimensional chemical transport model", J. Geophys. Res., **104**, 1781-1805, (1999)

## List of Figure Captions

**Fig. 1:** Light paths observed by an airborne UV/vis skylight absorption spectrometer (a) compared to the light paths observed by a ground-based UV/vis zenith sky absorption spectrometer (b). The displayed light paths indicate light paths taking into account single scattering only. In reality the light observed at a specific LOS originates from a variety of different light paths as a result of multiple scattering. The light gray layer represents a stratospheric and the dark gray layer represents a tropospheric trace gas layer.

**Fig. 2:** Averaging kernels for scenarios 1 through 6.

**Fig. 3:** Weighting functions for the scenarios 1, 2, 5, and 6. The  $\text{NO}_2$  profile is anticipated for mid-latitudes on the northern hemisphere in March at  $51.6^\circ$  SZA. Each weighting function corresponds to a different LOS. The magnitude of the weighting functions is small at the surface and above 15 km, revealing that the slant columns are not very sensitive to  $\text{NO}_2$  in these regions.

**Fig. 4:** Retrieval errors for scenarios 1, 2, 6, and 10.

**Fig. 5:** Averaging kernels for scenarios 6 and 7.

**Fig. 6:** Averaging kernels for scenarios 9 and 10.

**Fig. 7:** Pointing accuracy: a.) pointing error of  $-1^\circ$  for scenario 9, b.) pointing error of  $-0.5^\circ$  for scenario 10, c.) pointing error of  $-0.25^\circ$  for scenario 10, and d.) pointing error of  $-0.1^\circ$  for scenario 10. To characterize the decrease in quality of the retrieval the ratio of the retrieval error with and without pointing error is plotted.

Table 1. Scenarios for the sensitivity studies.

scenario	LOS [°]	flight			
		albedo $\lambda$ [nm]		altitude [km]	
	0, 60, 80, 85, 88,				
1	92, 95, 100, 120, 180	0.1	350	10	
2	see scenario 1	0.1	500	10	
3	see scenario 1	0.9	350	10	
4	see scenario 1	0.9	500	10	
	0, 80, 85, 88, 89,				
5	91, 92, 95, 100, 180	0.1	350	10	
6	see scenario 5	0.1	500	10	
7	see scenario 1	0.1	350	2	
8	see scenario 1	0.1	500	2	
9	see scenario 5 + 87, 93	0.1	350	10	
10	see scenario 5 + 87, 93	0.1	500	10	

Table 2. Vertical resolution (VR) of the considered sensitivity studies at 10 km flight altitude.

scenario	$\lambda$ [nm]	max. (min.) VR	
		below aircraft	above aircraft
		[km]	(<17 km) [km]
1	350	2.0 (4.9)	2.1 (4.9)
2	500	1.3 (4.6)	2.2 (5.5)
5	350	2.0 (4.8)	2.0 (5.6)
6	500	1.3 (4.2)	2.1 (5.5)
9	350	2.0 (4.7)	2.0 (6.0)
10	500	1.3 (2.3)	2.0 (5.5)



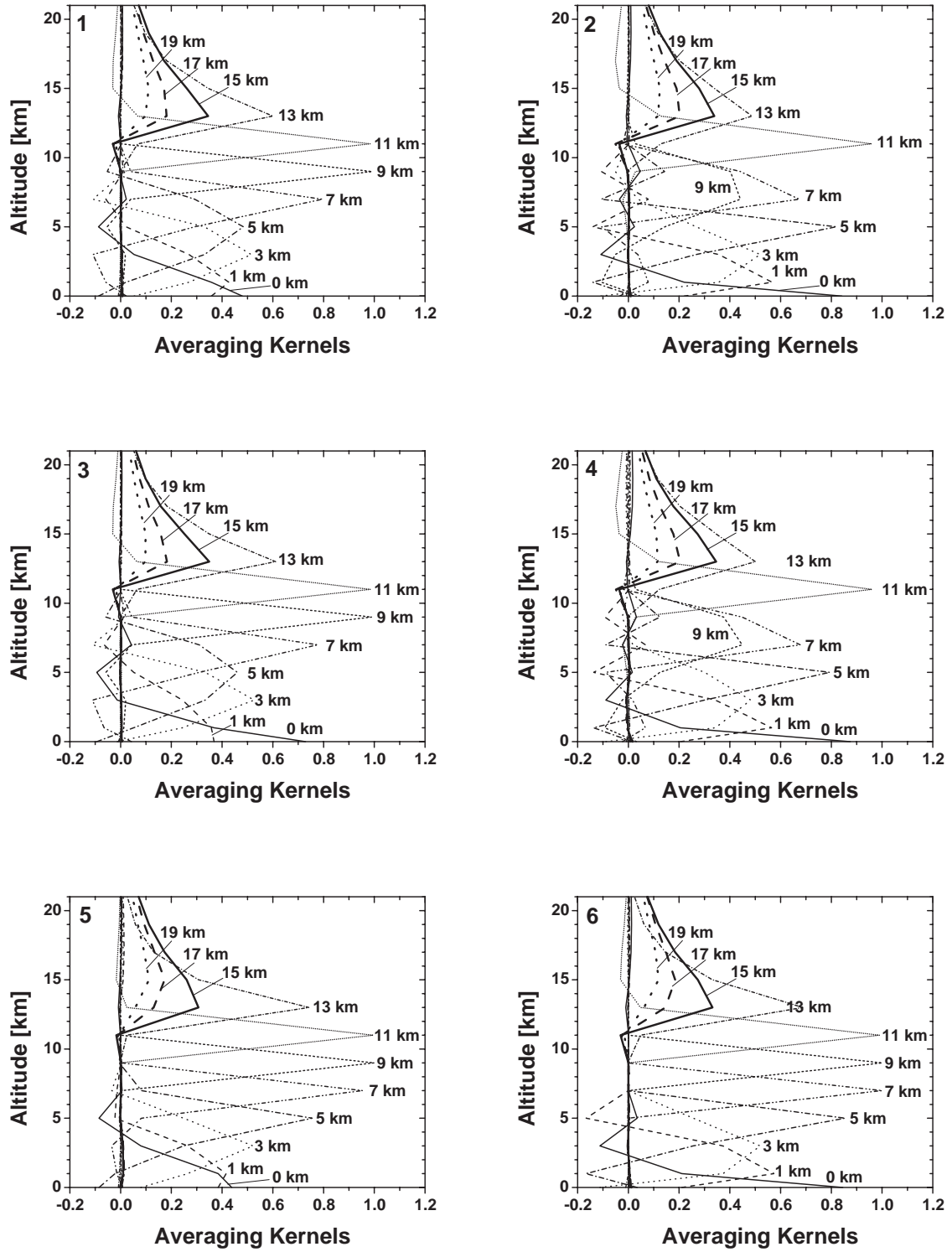


Fig. 2. Averaging kernels for scenarios 1 through 6.



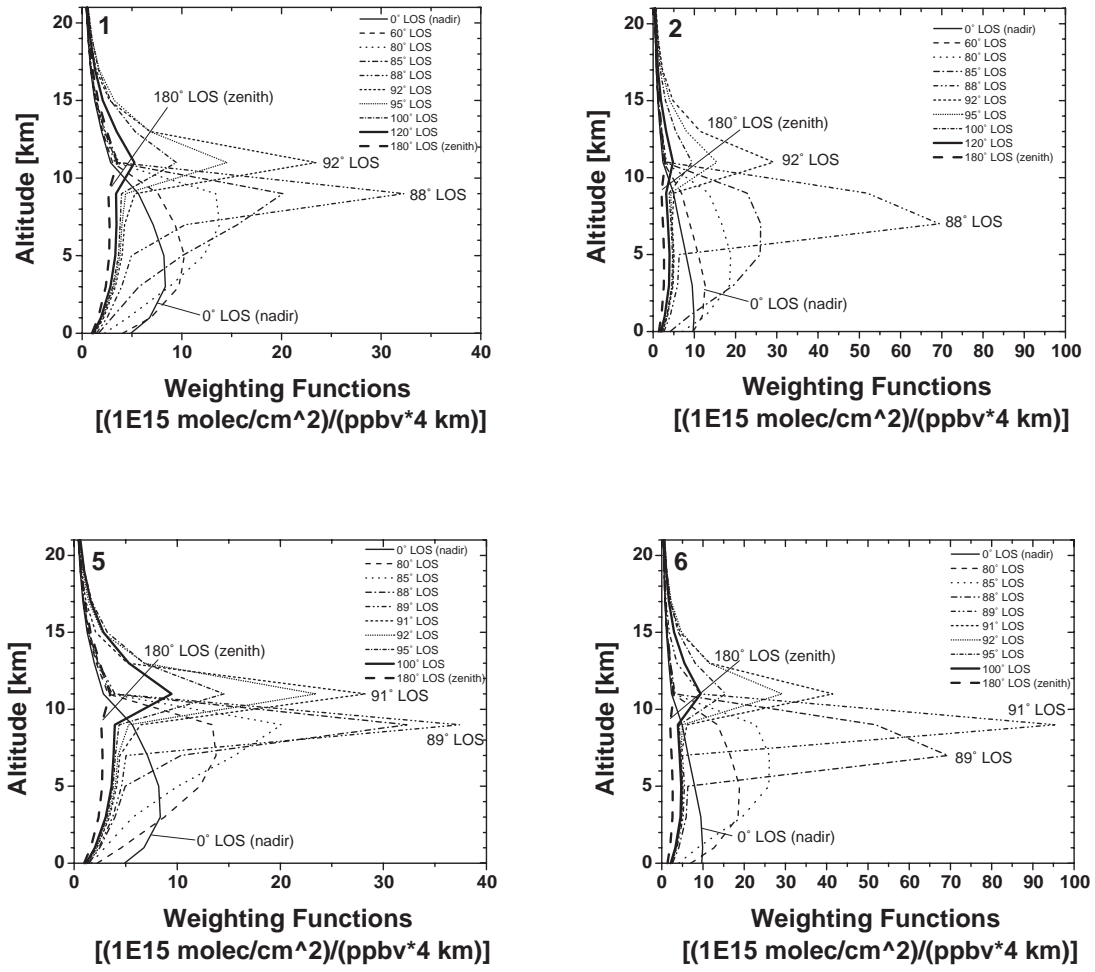


Fig. 3. Weighting functions for the scenarios 1, 2, 5, and 6. The NO<sub>2</sub> profile is anticipated for mid-latitudes on the northern hemisphere in March at 51.6° SZA. Each weighting function corresponds to a different LOS. The magnitude of the weighting functions is small at the surface and above 15 km, revealing that the slant columns are not very sensitive to NO<sub>2</sub> in these regions.

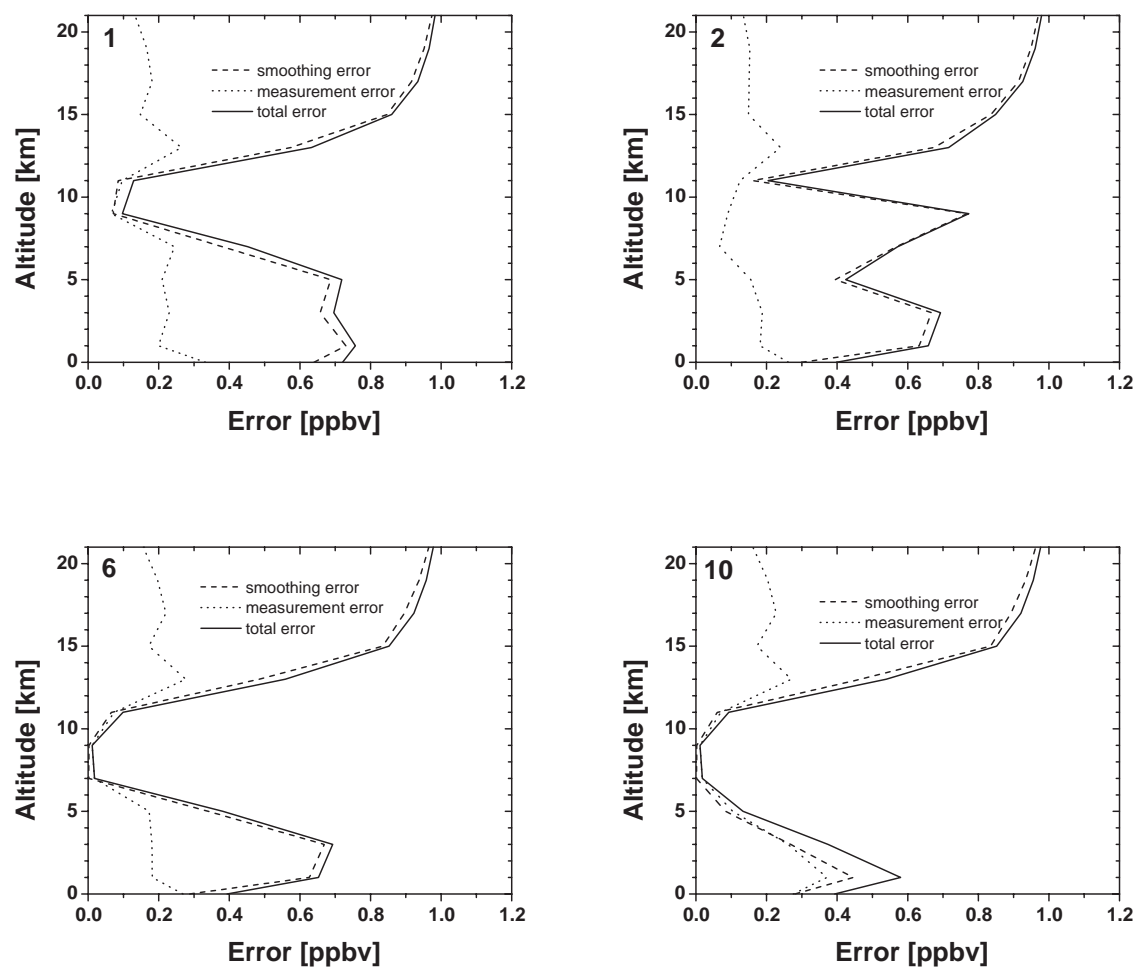


Fig. 4. Retrieval errors for scenarios 1, 2, 6, and 10.

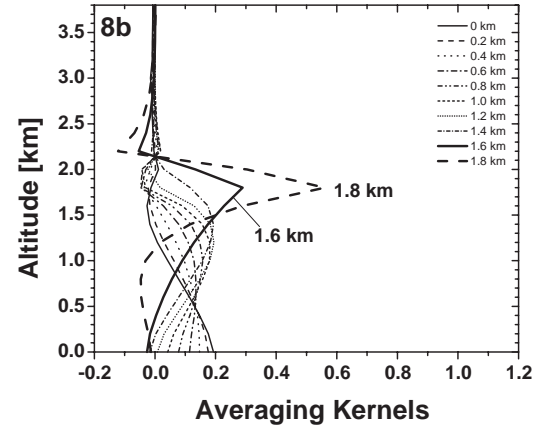
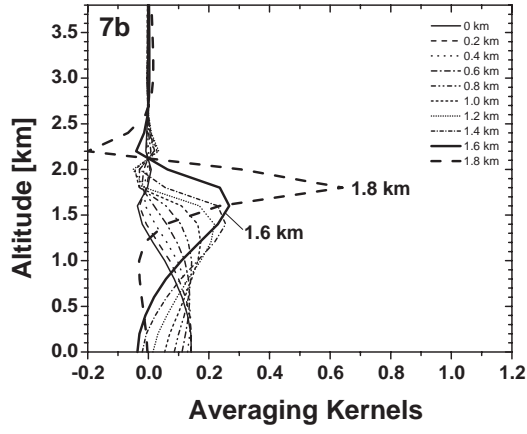
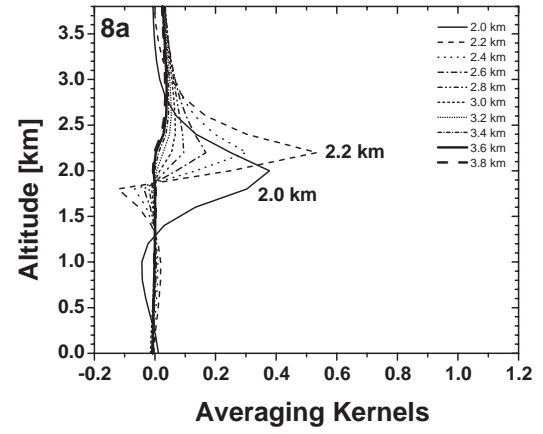
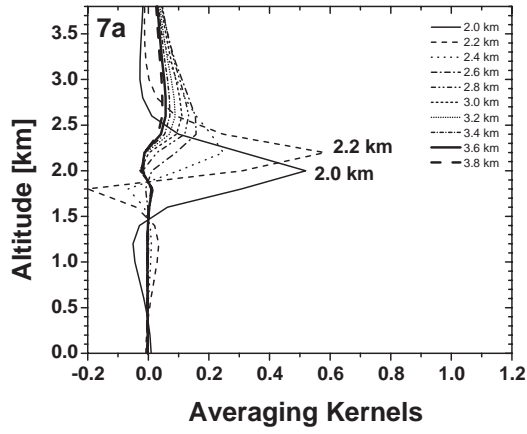


Fig. 5. Averaging kernels for scenarios 7 and 8.

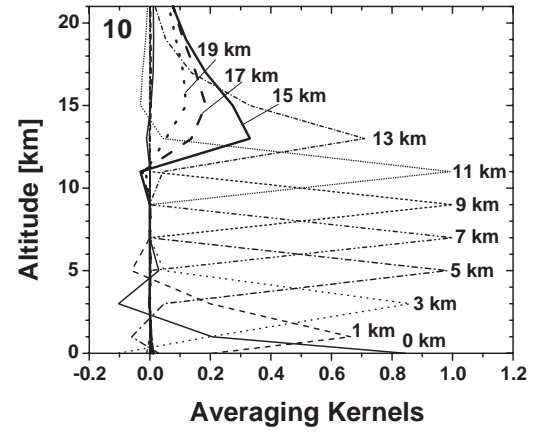
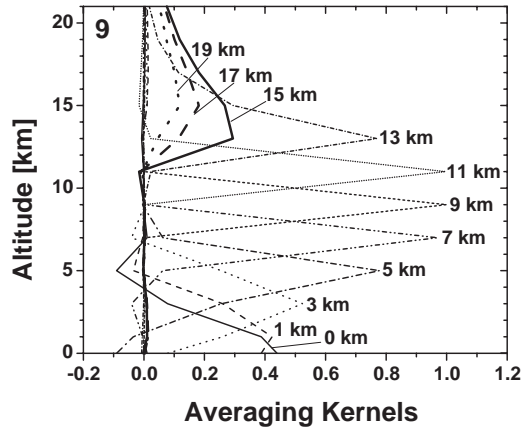


Fig. 6. Averaging kernels for scenarios 9 and 10.

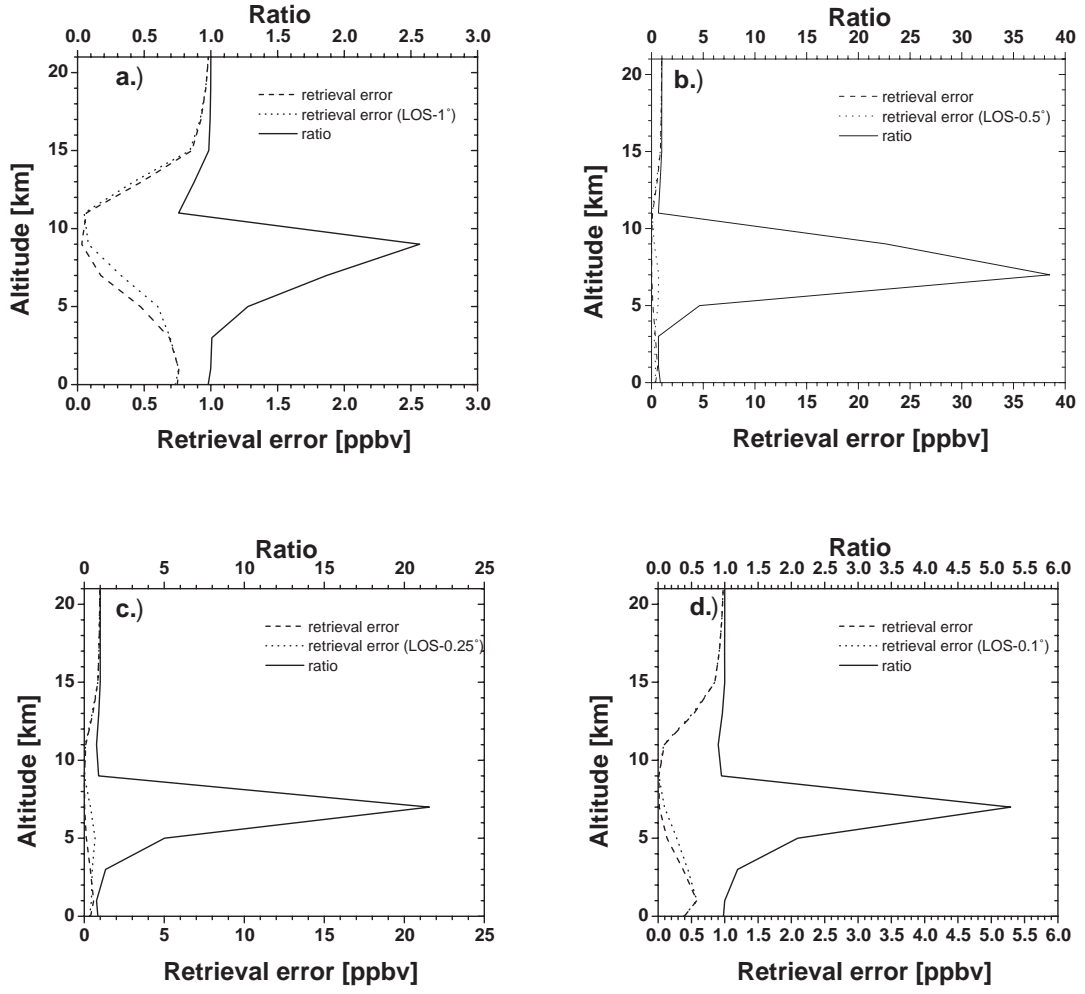


Fig. 7. Pointing accuracy: a.) pointing error of  $-1^\circ$  for scenario 9, b.) pointing error of  $-0.5^\circ$  for scenario 10, c.) pointing error of  $-0.25^\circ$  for scenario 10, and d.) pointing error of  $-0.1^\circ$  for scenario 10. To characterize the decrease in quality of the retrieval the ratio of the retrieval error with and without pointing error is plotted.